The iron exporter ferroportin/Slc40a1 is essential for iron homeostasis

Adriana Donovan,[1,2] Christine A. Lima,[1,3] Jack L. Pinkus,[4] Geraldine S. Pinkus,[4] Leonard I. Zon,[1,2,3] Sylvie Robine,[5] and Nancy C. Andrews[1,2,3,*]

[1]Children's Hospital Boston, Boston, Massachusetts 02115
[2]Harvard Medical School, Boston, Massachusetts, 02115
[3]Howard Hughes Medical Institute, Boston, Massachusetts 02115
[4]Department of Pathology, Brigham and Women's Hospital, Boston, Massachusetts 02115
[5]Equipe de Morphogenèse et Signalisation Cellulaires, Institut Curie, Paris, 75248, France
*Correspondence: nancy_andrews@hms.harvard.edu

Summary

Ferroportin (SLC40A1) is an iron transporter postulated to play roles in intestinal iron absorption and cellular iron release. Hepcidin, a regulatory peptide, binds to ferroportin and causes it to be internalized and degraded. If ferroportin is the major cellular iron exporter, ineffective hepcidin function could explain manifestations of human hemochromatosis disorders. To investigate this, we inactivated the murine *ferroportin* (*Fpn*) gene globally and selectively. Embryonic lethality of *Fpn*$^{null/null}$ animals indicated that ferroportin is essential early in development. Rescue of embryonic lethality through selective inactivation of *ferroportin* in the embryo proper suggested that ferroportin has an important function in the extraembryonic visceral endoderm. Ferroportin-deficient animals accumulated iron in enterocytes, macrophages, and hepatocytes, consistent with a key role for ferroportin in those cell types. Intestine-specific inactivation of ferroportin confirmed that it is critical for intestinal iron absorption. These observations define the major sites of ferroportin activity and give insight into hemochromatosis.

Introduction

Hereditary hemochromatosis is a disorder of iron homeostasis (Hentze et al., 2004). Homozygous mutations in any of four genes (*HFE*, *TFR2*, *hepcidin*, and *HJV*) result in similar phenotypes of varying severity (Camaschella et al., 2000; Feder et al., 1996; Papanikolaou et al., 2004; Roetto et al., 2003). Patients have pathological iron deposition in parenchymal cells of the liver, heart, pancreas, and other tissues. Paradoxically, macrophages retain less iron than in normal individuals. Understanding the pathogenesis of hemochromatosis requires insight into normal iron homeostasis and its perturbations in disease.

Mammalian iron homeostasis is maintained through complex regulation of tissues that transport, store, and utilize iron. Initial iron stores are established through maternoembryonic and maternofetal transfer. After birth, dietary iron is absorbed through enterocytes lining the duodenum. Iron circulates in the bloodstream bound to transferrin and is delivered to sites of utilization and storage. Erythroid precursors are the primary consumers, using iron to produce hemoglobin. Iron is recycled by tissue macrophages that phagocytose senescent erythrocytes and disassemble hemoglobin to return the metal to the circulation. Macrophage recycling is quantitatively important because the amount of iron supplied in this way is approximately 20-fold greater than the amount absorbed through the intestine on a daily basis (Hentze et al., 2004). Iron in excess of basal needs is stored in hepatocytes and macrophages. Unlike other metals, iron cannot be eliminated from the body through the liver or kidneys. Iron losses result from bleeding and exfoliation of skin and mucosal cells. Homeostasis functions to meet tissue iron needs while averting the toxicity of excess iron.

Iron homeostasis can be described in a simple manner by considering the actions of six cell types—extraembryonic visceral endodermal and placental cells that transfer iron from mother to fetus, absorptive enterocytes, erythroid precursors, recycling macrophages, and hepatocytes. The circulating pool of iron bound to transferrin is determined by the activities of these cells. These can be further categorized as epithelial cells that transfer iron across their apical and basolateral membranes (preplacental and placental cells, enterocytes), cells that store and release iron as needed (macrophages and hepatocytes), and cells that utilize iron but do not release it before they senesce (erythroid precursors).

Iron cannot pass through cellular membranes unassisted. To date, two transmembrane transporters have been identified—SLC11A2 (also known as DMT1, Nramp2, and DCT1) and ferroportin (also known as SLC40A1, IREG1, and MTP1) (Abboud and Haile, 2000; Donovan et al., 2000; Fleming et al., 1997; Gunshin et al., 1997; McKie et al., 2000). SLC11A2 acts as an iron importer, transporting iron into cells. Ferroportin acts as an iron exporter, transporting iron out of cells. Accordingly, in polarized epithelial cells, SLC11A2 is found on the apical membrane, and ferroportin is found on the basolateral membrane (Canonne-Hergaux et al., 1999; Donovan et al., 2000). SLC11A2 is also found in endosomes in erythroid precursors (Canonne-Hergaux et al., 2001; Fleming et al., 1998; Su et al., 1998), which use the transferrin cycle for iron uptake. Ferroportin is not expressed in erythroid cells but is present in the placenta, intestine, reticuloendothelial macrophages, and hepato-

cytes (Abboud and Haile, 2000; Donovan et al., 2000; McKie et al., 2000).

Studies of animals carrying loss-of-function mutations in *Slc11a2* suggested that it was the major if not the only transmembrane importer of nonheme iron (Fleming et al., 1997, 1998). In contrast, evidence for a major role for ferroportin in mammalian iron export has been indirect. Zebrafish embryos carrying mutations in a *ferroportin* ortholog have a defect in iron transfer from yolk sac to embryo (Donovan et al., 2000). Ferroportin has been shown to have iron export function when expressed in *Xenopus* oocytes (Donovan et al., 2000; McKie et al., 2000). The *ferroportin* mRNA contains an iron regulatory element in its 5′ untranslated region (Abboud and Haile, 2000; Donovan et al., 2000; Liu et al., 2002; McKie et al., 2000). Regulation of gene expression in intestine and macrophages is consistent with expectations for a major iron exporter (Knutson et al., 2003; McKie et al., 2000; Muckenthaler et al., 2003). In addition, perturbation of the *ferroportin* promoter region in mice causes transitory polycythemia (*pcm*/+) and iron deficiency anemia (*pcm*/*pcm*) (Mok et al., 2004). These observations are all suggestive, but none directly address the roles of ferroportin in normal iron homeostasis.

Formally, it was possible that hemochromatosis could result from aberrant regulation of iron import, iron export, or both. An important clue came from the discovery of hepcidin, a circulating peptide that has profound effects on iron absorption and distribution (Nicolas et al., 2001, 2002). Hereditary hemochromatosis is associated with inappropriately low hepcidin levels, either resulting from mutations in hepcidin itself or from mutations in genes that must, in some way, control hepcidin expression (Bridle et al., 2003; Kawabata et al., 2005; Muckenthaler et al., 2003; Nemeth et al., 2005; Nicolas et al., 2003; Papanikolaou et al., 2004; Roetto et al., 2003).

Recently, insight into hepcidin function came from the observation that hepcidin binds to ferroportin and targets it for destruction. The consequent hypothesis is that hemochromatosis results from unimpeded iron transport through ferroportin. Clinical findings could be explained by a greater transfer of iron from absorptive intestinal epithelial cells to the bloodstream and accelerated macrophage iron release. If this is correct, ferroportin must be the primary conduit for iron export from both types of cells. The experiments described in this report test that interpretation and provide confirmation that it is correct.

The role of ferroportin in vivo has been confounded by the finding that mutations in *ferroportin* occur in a subset of human patients with iron overload. Individuals heterozygous for a variety of missense mutations in *ferroportin* develop macrophage-predominant iron overload that may progress to iron-induced organ damage (Montosi et al., 2001; Njajou et al., 2001; Pietrangelo, 2004). This has been referred to as autosomal dominant hemochromatosis or, more accurately, "ferroportin disease" (Pietrangelo, 2004). If it is true that ferroportin plays important roles in both enterocytes and macrophages, there is no simple loss-of-function or gain-of-function model to explain this disorder. Gain-of-function mutations might lead to the increased intestinal iron absorption observed in patients with autosomal dominant ferroportin disease but would not account for macrophage iron loading. Loss-of-function mutations would explain the large amount of iron observed in patient macrophages but would not readily account for increased intestinal iron absorption. A hypothesis has been set forth to reconcile this—that macrophage iron retention leads to iron-restricted erythropoiesis, and a compensatory augmentation of intestinal absorption overcomes haploinsufficiency of ferroportin in enterocytes. In support of this hypothesis, some patients have been reported to have anemia early in the course of their disease.

Table 1. Analysis of offspring from intercrosses of *Fpn1*$^{null/+}$ animals

Age	*Fpn*$^{+/+}$	*Fpn*$^{null/+}$	*Fpn*$^{null/null}$	Resorbed	Total
E7.5	5	7	1	3	16
E8.5	2	4	1	5	12
E9.5	7	9	0	6	22
>E10.5	10	21	0	9	40
Total	24	41	2	23	90
%	26.7	45.6	2.2	25.6	
Postnatal	65	85	0		150

We sacrificed and dissected pregnant mothers at different times postfertilization. At each time point, we counted the total number of embryonic sacs present in the uterus. Subsequently, each sac was dissected to reveal the embryo. Sacs that were empty were categorized as resorbed. Each embryo was developmentally staged according to Theiler (1989). The total numbers of embryos of each genotype (*Fpn*$^{+/+}$, *Fpn*$^{null/+}$, and *Fpn*$^{null/null}$) and the total number of resorbed embryos were counted for each developmental stage. The genotypes of animals from live births are summarized at the bottom of the table.

The purposes of this study were to determine which cell types are dependent upon ferroportin function and to directly test the hypothesis that ferroportin disease results from heterozygous loss-of-function mutations in *ferroportin*. We took advantage of strong similarities between murine and human iron metabolism (Andrews, 2000). We inactivated the murine *ferroportin* gene globally and in selected tissues, through gene targeting and homologous recombination in pluripotential embryonic stem cells. Our studies show that ferroportin is required for both prenatal and postnatal iron homeostasis. Specifically, we find that ferroportin is required for iron transfer in the extraembryonic visceral endoderm and for iron export from enterocytes, macrophages, and hepatocytes.

Results

Targeted disruption of *ferroportin* results in embryonic lethality

To generate a *ferroportin* (*Fpn*) knockout allele, we replaced exon 6 and part of exon 7 (amino acids 172–338) with a neomycin resistance cassette using homologous recombination in J1 embryonic stem (ES) cells (see Figure S1A with the Supplemental Data available with this article online). This knockout strategy deletes sequence that encodes three of the ten predicted transmembrane segments of the ferroportin protein. We identified correctly targeted clones by Southern blot analysis. We injected targeted ES cells into blastocysts to obtain chimeric animals, which were bred with 129/SvEvTac females to produce F1 offspring carrying the modified *ferroportin* allele. We confirmed germline transmission of the targeted allele by Southern blot analysis (Figure S1B). Animals carrying the targeted allele will be referred to as *Fpn*$^{null/+}$ or *Fpn*$^{null/null}$.

We interbred *Fpn*$^{null/+}$ animals in an attempt to produce *Fpn*$^{null/null}$ offspring. However, we obtained no *Fpn*$^{null/null}$ animals among 150 pups genotyped, indicating that *Fpn*$^{null/null}$ animals died prenatally (Table 1). We determined that most

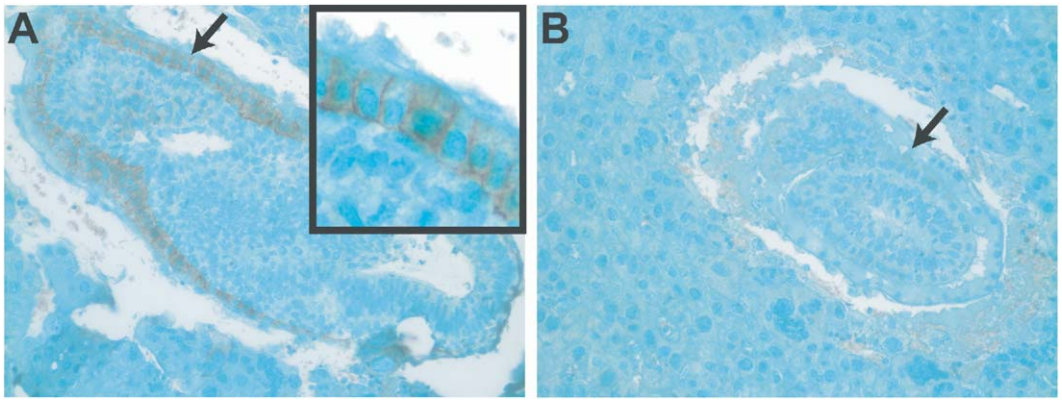

Figure 1. Embryonic expression of ferroportin protein

Immunohistochemical staining for ferroportin in a wild-type E7.0 embryo (**A**). The brown staining indicates the expression of ferroportin in the extraembryonic visceral endoderm (arrow). At higher power ([**A**], inset), it is evident that these cells are a polarized epithelium with ferroportin expressed on the basolateral surface, as it is in duodenal enterocytes of the intestine. A littermate of the embryo in (**A**) that appears significantly smaller and has no detectable ferroportin protein by immunohistochemistry (**B**). The arrow points to the extraembryonic visceral endoderm.

Fpn$^{null/null}$ animals die by E7.5. However, we were able to identify one *Fpn*$^{null/null}$ embryo at E7.5 and one at E8.5 (Table 1). We reproduced these results in animals carrying a targeted *ferroportin* allele from which the neomycin cassette had been removed (data not shown).

Role for ferroportin in extraembryonic visceral endoderm

We hypothesized that *Fpn*$^{null/null}$ embryos died from a defect in iron transfer from the mother. The extraembryonic visceral endoderm (exVE) functions in maternoembryonic nutrient transport prior to placenta formation (Bielinska et al., 1999). We examined the expression of ferroportin in early embryos by immunohistochemistry. In wild-type embryos, ferroportin was strongly expressed at the basolateral membrane of polarized epithelial cells in the exVE (Figure 1A). Analogous studies of littermates from intercrosses of *Fpn*$^{null/+}$ animals identified embryos with no ferroportin expression in the exVE (Figure 1B). These animals were significantly smaller than their ferroportin-expressing littermates and were presumed to be *Fpn*$^{null/null}$ embryos. Considering the known function of ferroportin in cellular iron export, it appears that *Fpn*$^{null/null}$ embryos cannot transfer iron from the exVE into the embryo proper, leading to a defect in embryonic growth and consequent death.

Fpn$^{null/+}$ animals have a mild disruption of iron homeostasis

Although *Fpn*$^{null/null}$ animals died early in development, *Fpn*$^{null/+}$ animals were viable. If simple loss-of-function mutations in *ferroportin* cause autosomal dominant iron overload in the human disease, then *Fpn*$^{null/+}$ mice should be a model of that disorder. To test this hypothesis, we analyzed parameters of iron homeostasis in *Fpn*$^{null/+}$ animals as compared to wild-type littermates. At age 3 months, *Fpn*$^{null/+}$ animals were indistinguishable from controls in all measurements. However, by age 6 months, we detected evidence of disrupted iron homeostasis in *Fpn*$^{null/+}$ animals. *Fpn*$^{null/+}$ mice were not anemic, but both reticulocytes and mature erythrocytes had decreased cellular hemoglobin and decreased cell volume, indicative of iron-restricted erythropoiesis. The erythrocyte cellular hemoglobin content was 15.0 ± 0.2 pg in *Fpn*$^{+/+}$ males (n = 9) and 14.1 ± 0.2 pg in *Fpn*$^{null/+}$ males (n = 5). The difference was highly significant (p value $\leq$ 0.00001). The erythrocyte mean cell volume was 51.4 ± 0.9 fL in *Fpn*$^{+/+}$ males (n = 9) and 48.7 ± 1.4 fL in *Fpn*$^{null/+}$ males (n = 5) (p value $\leq$ 0.01). Six-month-old *Fpn*$^{null/+}$ male mice also had significantly less nonheme iron in the liver and showed a trend toward lower spleen iron when compared to wild-type littermates (liver: *Fpn*$^{null/+}$ 158.8 ± 64.9 μg/g, *Fpn*$^{+/+}$ 243.3 ± 45.8 μg/g, p value $\leq$ 0.04; spleen: *Fpn*$^{null/+}$ 1656.8 ± 411.8 μg/g, *Fpn*$^{+/+}$ 2085.3 ± 449.1 μg/g, p value = 0.1).

We considered the possibility that more time was needed for the iron-loading phenotype to develop. At age 12 months, *Fpn*$^{null/+}$ mice continued to have significantly lower erythrocyte cellular hemoglobin and mean cell volume as compared to wild-type littermates (data not shown). In addition, liver iron content remained lower in *Fpn*$^{null/+}$ mice (116.2 ± 26.8 μg/g, n = 20) than in *Fpn*$^{+/+}$ littermates (178.3 ± 33.1 μg/g, n = 14) (p value $\leq$ 0.00001). However, spleen iron content in *Fpn*$^{null/+}$ animals was greater (2259.24 ± 392.9 μg/g, n = 20) than in *Fpn*$^{+/+}$ animals (1797.16 ± 289.6 μg/g, n = 14) (p value $\leq$ 0.0005).

Most nonheme iron in the spleen is contained in macrophages, while nonheme iron in the liver is contained in both hepatocytes and macrophages. At 1 year of age, increased splenic iron suggests that iron is being retained in macrophages in *Fpn*$^{null/+}$ animals to a greater degree than in wild-type controls. This is similar to the human iron overload disease due to ferroportin mutations. However, in contrast to human patients, hepatic iron stores were diminished. Thus, our data suggest that *Fpn*$^{null/+}$ mice are not a faithful model of the human disease.

Conditional disruption of *ferroportin*

In order to study the role of ferroportin in adult mouse tissues, we retargeted the *ferroportin* locus and introduced LoxP sites into introns flanking exons 6 and 7 to generate a "floxed" allele (Figure S1A). We refer to mice that are homozygous for the floxed allele as *Fpn*$^{flox/flox}$. In the presence of Cre recombinase, sequences between the LoxP sites can be excised. This condi-

tional knockout strategy deletes sequence that encodes six of the ten predicted transmembrane segments of the ferroportin protein.

Ferroportin is required for iron homeostasis after birth

To circumvent embryonic lethality due to loss of ferroportin in tissues involved in maternoembryonic iron transfer, we bred *Fpn*$^{flox/flox}$ animals to *Meox2-Cre* mice (Tallquist and Soriano, 2000). *Meox2-Cre;Fpn*$^{flox/flox}$ mice should express Cre recombinase and inactivate *ferroportin* in all tissues except exVE and placenta. *Meox2-Cre;Fpn*$^{flox/flox}$ mice were born alive and initially appeared identical to their wild-type littermates. However, within the first few days of life, they were noted to be pale and runted. By P10–P12, the difference between wild-type and mutant animals was pronounced (Figure 2A). We observed variability in both the onset and severity of the phenotype, likely due to incomplete Cre-mediated excision in some animals. Accordingly, genotyping of animals with severe phenotypes demonstrated complete or near-complete excision of the floxed allele in all tissues and organs examined, whereas excision was incomplete in animals with milder phenotypes (data not shown).

Meox2-cre;Fpn$^{flox/flox}$ mice were anemic, explaining their pallor. Blood smears revealed hypochromia, anisocytosis, poikilocytosis, and reticulocytosis (Figures 2B and 2C), similar to other mouse mutants with severe iron deficiency anemia. Measurement of erythrocyte parameters revealed decreased total hemoglobin, mean cell volume, and mean cell hemoglobin in both reticulocytes and mature erythrocytes (Table S1). The red cell distribution width and reticulocyte count were increased. These data strongly support the conclusion that the anemia in *Meox2-Cre*;*Fpn*$^{flox/flox}$ mice resulted from iron deficiency.

We examined tissues suspected to require ferroportin function including duodenum, liver, and spleen. Because ferroportin functions as an iron exporter, loss of its activity should result in cellular iron retention, demonstrable by histochemical stains that detect nonheme iron. We compared tissues from *Meox2-Cre*;*Fpn*$^{flox/flox}$ mice and wild-type littermates. Wild-type animals had no stainable nonheme iron in duodenal enterocytes (Figure 3A). In contrast, *Meox2-Cre*;*Fpn*$^{flox/flox}$ mice had abundant enterocyte iron (Figure 3B), suggesting that iron taken up from the diet or plasma cannot be exported across the basolateral membrane into the circulation. Considering the substantial requirement for efficient dietary iron absorption to support growth in the first 3 weeks of life, this intestinal defect might, by itself, explain the development of iron deficiency anemia in the mutant animals.

We also examined tissue sections from the liver and spleen. Wild-type liver samples showed no detectable iron in hepatocytes or Kupffer cells at age 12 days. In contrast, *Meox2-Cre*;*Fpn*$^{flox/flox}$ mice showed pronounced iron accumulation in Kupffer cells, the resident macrophages of the liver, and in hepatocytes (Figures 3C and 3D). We also observed considerable iron accumulation in splenic macrophages of *Meox2-Cre*;*Fpn*$^{flox/flox}$ mice but not controls (Figures 3E and 3F). These observations support the hypothesis that ferroportin is important for export of iron from both macrophages and hepatocytes.

We measured nonheme tissue iron content. *Meox2-Cre*;*Fpn* mutant animals sacrificed at 10–12 days of age had 2.3- and 1.7-fold more nonheme iron in liver and spleen, respectively, as compared to their wild-type littermates (Figure 4), consistent with the histochemical staining. At 18–22 days of age, *Meox2-Cre*;*Fpn* mutant animals continued to have higher spleen iron (4.4-fold), but their liver iron content was 1.7-fold lower than their wild-type littermates (Figure 4). This pattern is most likely explained by the overall iron deficiency of these animals. The

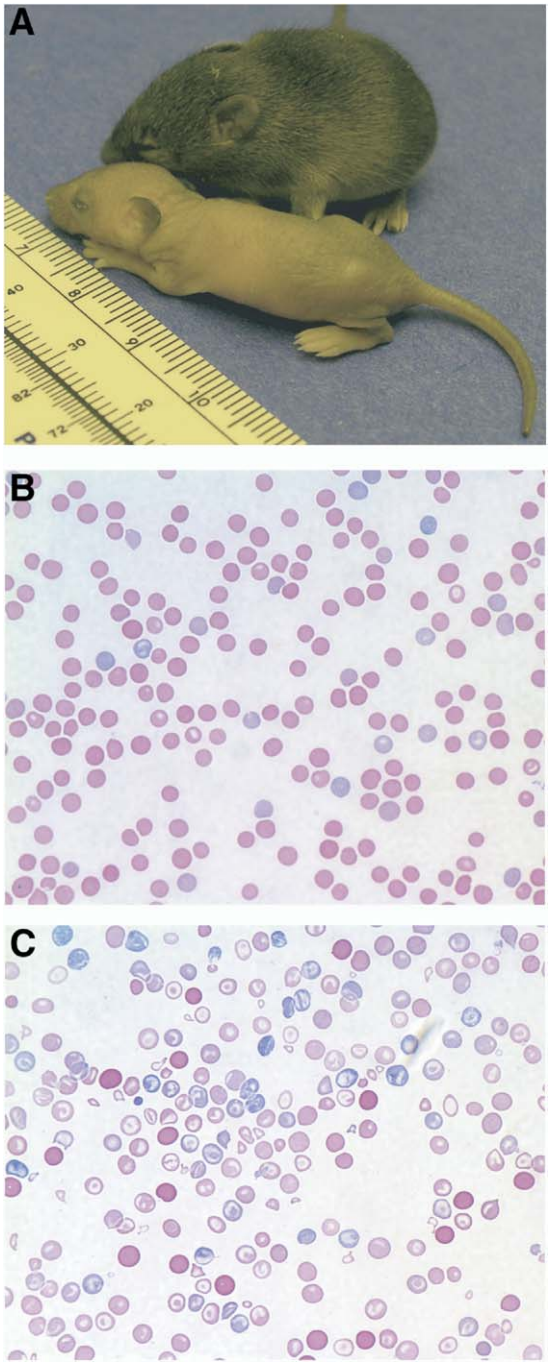

Figure 2. Conditional deletion of *ferroportin* by *Meox2-Cre* causes iron deficiency anemia

The 10-day-old *Meox2-cre;Fpn1*$^{flox/flox}$ pup ([**A**], bottom) is small and pale compared to a wild-type littermate ([**A**], top). Peripheral blood smear of a 12-day-old wild-type animal stained with Wright-Giemsa (**B**). Peripheral blood smear of a 12-day-old *Meox2-Cre;Fpn1*$^{flox/flox}$ animal stained with Wright-Giemsa (**C**).

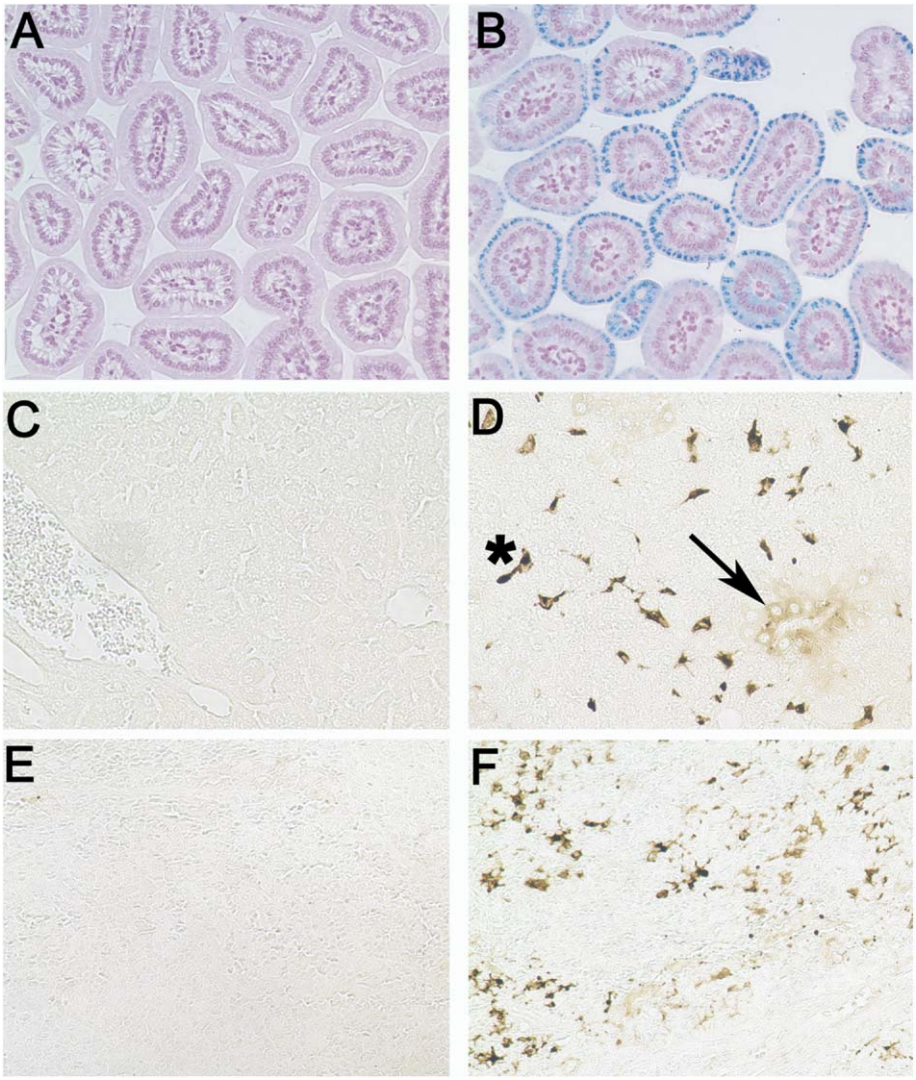

Figure 3. *Meox2-Cre;Fpn* mutant mice accumulate iron in enterocytes, macrophages, and hepatocytes

Perls Prussian blue stain for iron in crosssections of duodenal villi of 12-day-old mice (**A** and **B**). Blue staining shows iron accumulated in enterocytes. DAB-enhanced Perls stain for iron in liver sections from 12-day-old mice (**C** and **D**). Brown staining shows iron accumulated in cells. The asterix (*) marks a Kupffer cell, and the arrow points to hepatocytes that are loaded with iron. DAB-enhanced Perls stain for iron in spleen sections of 12-day-old mice (**E** and **F**). The genotypes of the mice are the following: $Fpn^{flox/flox}$ (**A**, **C**, and **E**) and *Meox2-Cre;* $Fpn^{flox/flox}$ (**B**, **D**, and **F**).

liver continues to grow in size with increasing age, but iron-deficient animals cannot deposit additional iron in hepatocytes, eventually leading to a decrease in liver iron content.

Ferroportin is important in intestinal iron absorption

We wanted to develop mice expressing ferroportin in all tissues except the intestine in order to distinguish the role of the protein in the intestine from its roles in other cell types. Initially, we bred $Fpn^{flox/flox}$ animals to mice expressing Cre recombinase under the control of the villin promoter (el Marjou et al., 2004). In adult animals, villin expression is highly restricted to the intestine and, to a lesser extent, the kidney. However, similar to our first, global knockout model, no *ferroportin*-deleted mice were born. Because intestinal ferroportin should not be required before birth, we suspected that the villin-Cre transgene was also expressed in the exVE, resulting in early deletion of ferroportin and embryonic death. Subsequent studies confirmed that the villin promoter directs expression of Cre recombinase in exVE (el Marjou et al., 2004).

To bypass this problem, we bred $Fpn^{flox/flox}$ mice to mice carrying an intestine-restricted villin-Cre transgene that is inducible by tamoxifen (el Marjou et al., 2004). The resulting *vil-Cre-*ER^{T2};$Fpn^{flox/flox}$ mice should be born with *ferroportin* alleles intact. However, after administration of tamoxifen, Cre recombinase causes tissue-specific inactivation of *ferroportin*.

We administered tamoxifen to *vil-Cre-*ER^{T2};$Fpn^{flox/flox}$ and $Fpn^{flox/flox}$ mice starting at age 1 week. We confirmed by both PCR and Southern blot analyses that inactivation of ferroportin occurred exclusively in the intestine (Figure 5A and data not shown). Approximately 50% of the total DNA in a duodenal segment showed *ferroportin* deletion. Based on earlier characterization of the *vil-Cre-*ER^{T2} mouse model, it is likely that the observed 50% deletion in whole intestine corresponds to 100% deletion in crypt cells and enterocytes, with no deletion in nonepithelial cell types (el Marjou et al., 2004). In order to confirm that ferroportin was not expressed in *vil-Cre-*ER^{T2};$Fpn^{flox/flox}$ mice, we performed immunohistochemistry with an anti-ferroportin antibody. Ferroportin is clearly expressed on the basolateral surface of enterocytes in the duodenum of $Fpn^{flox/flox}$ mice, but is absent in *vil-Cre-*ER^{T2};$Fpn^{flox/flox}$ mice (Figures 5B and 5C).

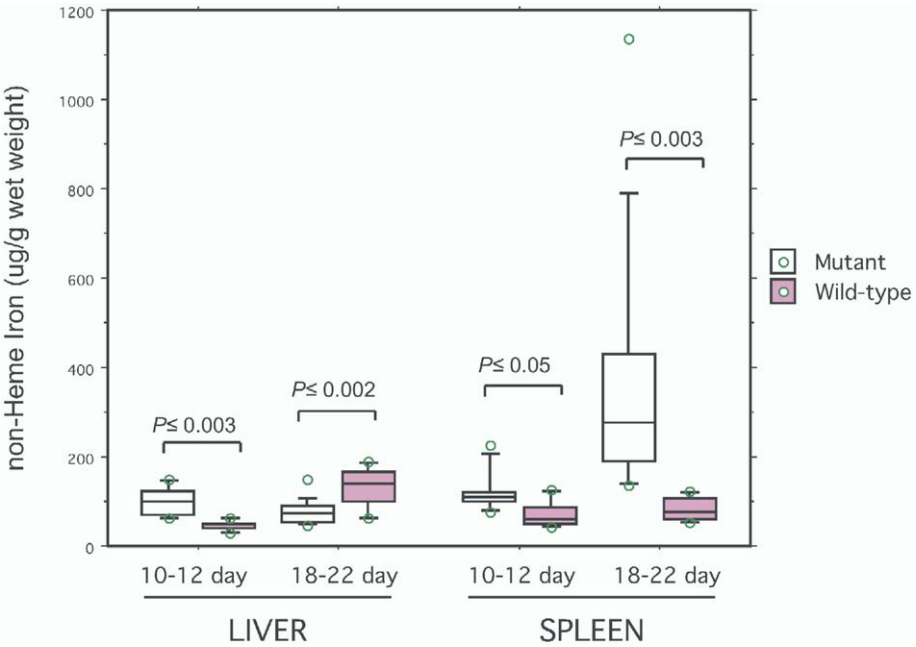

Figure 4. *Meox2-Cre;Fpn* mutant mice have abnormal nonheme iron levels in liver and spleen

Box plot depicting the measurement of nonheme iron levels (μg Fe/g wet weight) in liver and spleen of wild-type controls (pink boxes) and *Meox2-Cre*; *Fpn* mutants (white boxes). The genotypes of the *Meox2-Cre*;*Fpn* mutant mice were *Meox2-Cre;* $Fpn^{flox/flox}$ and *Meox2-Cre*;$Fpn^{flox/null}$. The genotypes of the wild-type controls were $Fpn^{flox/flox}$, $Fpn^{flox/+}$, and $Fpn^{flox/null}$. We analyzed animals at two different ages: (1) 10- to 12-day-old mice (wild-type n = 6 and mutant n = 7) and (2) 18- to 22-day-old mice (wild-type n = 13 and mutant n = 11). This data was collected from both male and female animals. p values were calculated using Student's T-test. The box plot was drawn using Statview 5.0.1 (SAS Institute, Inc.) The middle bar of the box represents the median. The top of the box is the 75th percentile of the data set, and the bottom of the box is the 25th percentile. The top whisker represents the 90th percentile of the data, and the bottom whisker represents the 10th percentile of the data. The circles represent data points that lie outside of the 10th and 90th percentiles.

The *vil-Cre-*ER^{T2};$Fpn^{flox/flox}$ mice were visibly anemic as early as 8 days after the first tamoxifen injection. At 6–7 weeks of age, peripheral blood smears were consistent with severe iron deficiency anemia (Figures 6A and 6B). The average hematocrit of *vil-Cre-*ER^{T2};$Fpn^{flox/flox}$ animals was 11.2% ± 1.6% (n = 9), compared to 45.3% ± 5.9% (n = 11) in $Fpn^{flox/flox}$ controls (p value ≤ 0.00001). The average hemoglobin concentration of mutant mice was 2.8 ± 0.6 g/dl (n = 9), compared to 13.8 ± 1.8 g/dl (n = 11) in wild-type littermates (p value ≤ 0.00001). The duodenal enterocytes of *vil-Cre-*ER^{T2};$Fpn^{flox/flox}$ animals showed marked iron accumulation (Figures 6C and 6D). However, there was no stainable iron in the liver or spleen of *vil-Cre-*ER^{T2};$Fpn^{flox/flox}$ animals (data not shown). The *vil-Cre-*ER^{T2};$Fpn^{flox/flox}$ mice had 4.7-fold less nonheme iron in liver and 5.5-fold less nonheme iron in spleen as compared to their $Fpn^{flox/flox}$ littermates (liver: *vil-Cre-*ER^{T2};$Fpn^{flox/flox}$ 23.0 ± 3.9 μg/g, $Fpn^{flox/flox}$ 106.9 ± 6.3 μg/g, p value ≤ 0.0003; spleen: *vil-Cre-*ER^{T2};$Fpn^{flox/flox}$ 27.0 ± 5.8 μg/g, $Fpn^{flox/flox}$ 148.3 ± 25.9 μg/g, p value ≤ 0.013). This severe iron deficiency is consistent with an important role for ferroportin in intestinal iron absorption. When ferroportin is inactivated exclusively in the intestine but intact in other tissues, iron is not retained in macrophages and hepatocytes, consistent with an appropriate response to iron deficiency.

If anemia and iron deficiency in *vil-Cre-*ER^{T2};$Fpn^{flox/flox}$ animals result from a block in intestinal iron absorption, it should be possible to restore normal iron balance through parenteral treatment with iron dextran. Accordingly, after administration of iron dextran, the hematocrits of *vil-Cre-*ER^{T2};$Fpn^{flox/flox}$ mice returned to normal within 1 week. The hematocrits of $Fpn^{flox/flox}$ animals before and after treatment ranged from 46% to 49%. Before treatment, the hematocrits of *vil-Cre-*ER^{T2};$Fpn^{flox/flox}$ animals ranged from 9% to 11%. One week later, untreated *vil-Cre-*ER^{T2};$Fpn^{flox/flox}$ mice still had a mean hematocrit of 8.9% ± 2.2% (n = 3), while the iron dextran-treated *vil-Cre-*ER^{T2};$Fpn^{flox/flox}$ mice had a mean hematocrit of 41.7% ± 4.5% (n = 3) (p value ≤ 0.002). These results confirm that ferroportin is critical for intestinal absorption of iron.

Discussion

Our findings indicate that ferroportin is the major (if not only) basolateral iron exporter functioning in epithelial cells of the exVE and the intestine. When *ferroportin* is inactivated globally, there is an early failure in embryonic development, likely due to iron insufficiency. When it is preserved in the exVE and placenta but inactivated in all other tissues, prenatal development proceeds normally, but iron deficiency ensues rapidly after birth, when the intestine becomes the only route for iron entry.

Selective inactivation of *ferroportin* in postnatal intestine resulted in severe iron deficiency that was corrected by parenteral administration of iron, confirming that ferroportin function is necessary for dietary iron absorption in mice. While it remains possible that there are alternative, minor pathways for enterocyte iron export, the severity of the phenotype suggests that none can substitute for the activity of ferroportin.

The requirement for ferroportin activity in the intestine has additional implications for iron homeostasis. The undifferentiated crypt cells that develop into enterocytes, and perhaps the enterocytes themselves, acquire iron from the circulation (Bedard et al., 1976). The amount of plasma iron entering these cells is not insignificant, because the surface area of the villous epithelium is immense. If export of iron is interrupted, the flow of iron into this compartment becomes unidirectional. Enterocytes have a limited lifespan—after several days, they senesce and are sloughed into the gut lumen, resulting in loss of any iron they contain. Thus, we would expect that animals lacking intestinal ferroportin function would not only have a defect in iron absorption—they would also have increased iron losses.

While it has been assumed that there is no regulated iron

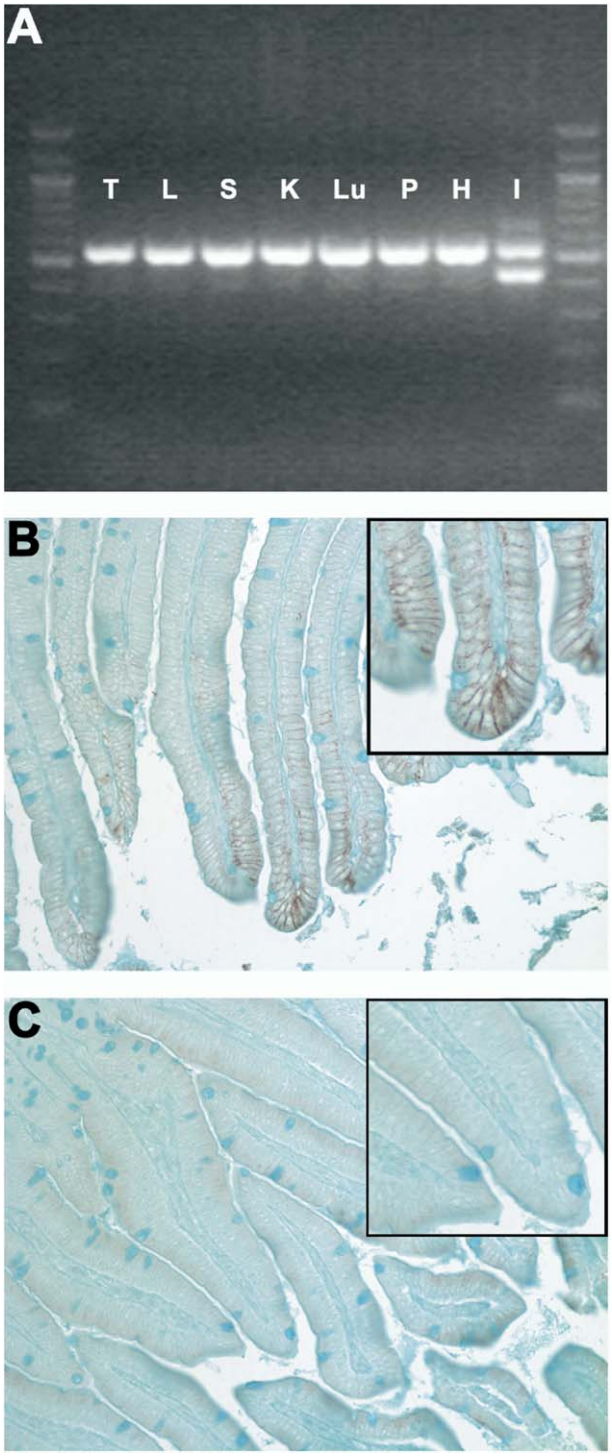

Figure 5. Conditional deletion of *ferroportin* in enterocytes by *vil-Cre-ER*^{T2}

PCR analysis of tissue DNA from a *vil-Cre-ER*^{T2};*Fpn*$^{flox/flox}$ mouse that was injected with tamoxifen (**A**). Tail (T), liver (L), spleen (S), kidney (K), lung (Lu), pancreas (P), heart (H), intestine (I). The marker is a 100 bp ladder. The floxed allele is 522 bp, and the full deletion allele is 398 bp. Immunohistochemistry for ferroportin protein in a wild-type animal (**B**) and a *vil-Cre-ER*^{T2};*Fpn*$^{flox/flox}$ mouse injected with tamoxifen (**C**). Brown staining represents ferroportin expression in duodenal enterocytes. Higher magnification images show basolateral localization of ferroportin in the wild-type animals ([**B**], inset) and absence of ferroportin expression in the *vil-Cre-ER*^{T2};*Fpn*$^{flox/flox}$ mouse ([**C**], inset).

excretion because neither the liver nor the kidney efficiently releases iron from the body, our results suggest that iron loss could be regulated at a different level. In iron deficiency, increased ferroportin expression would not only ensure increased intestinal absorption but also allow for maximal recovery of iron that has entered the intestinal epithelium from the plasma. On the other hand, decreased ferroportin expression in iron overload could augment normal iron losses by increasing the amount of iron contained in exfoliated enterocytes. Thus, regulation of ferroportin might be considered a novel mechanism of regulating iron "excretion." This need not occur through a mechanism that regulates the production of ferroportin. Indeed, *hepcidin* can exert control of ferroportin by modulating protein levels (Nemeth et al., 2004). This homeostatic mechanism allows regulation of intestinal iron absorption in response to iron availability and needs elsewhere in the body.

We have shown that ferroportin also plays important roles in nonepithelial cells. Global inactivation of *ferroportin* resulted in other perturbations of cellular iron distribution. Macrophages of the liver and spleen showed marked iron retention, likely because they had phagocytosed effete erythrocytes but had no mechanism for releasing recovered iron. Hepatocytes also appeared to retain the iron that they had acquired prenatally. These observations suggest that, as in enterocytes, ferroportin is the major iron exporter functioning in iron-recycling macrophages and hepatocytes. Iron retention by those cells undoubtedly compounds the effects of inadequate iron absorption, further depriving erythroid precursors of iron for hemoglobin production and thus exacerbating the anemia.

Few other cell types need to have an iron export function. However, iron transfer across the blood-brain barrier does require a cellular export step. We have not directly addressed the role of ferroportin in the brain in this study. However, in a separate study, we bred with mice expressing Cre recombinase under the control of a nestin promoter (Tronche et al., 1999) and did not note any gross behavioral abnormalities that might be attributed to cerebral or cerebellar dysfunction (data not shown).

Mice heterozygous for *ferroportin* mutations have a subtle phenotype that is not measurable before 6 months of age. Similar to human patients with autosomal dominant ferroportin disease, they accumulated iron in tissue macrophages and showed mild evidence of iron-restricted erythropoiesis. However, even at 1 year of age, they did not appear to have increased liver iron that would have been indicative of total body iron overload.

There are several possible explanations for the differences between *Fpn*$^{null/+}$ mice and human patients. First, it might be that clinical iron overload requires more time, and 1 year is not long enough for it to become manifest. This seems unlikely, because liver iron content was consistently decreased in *Fpn*$^{null/+}$ mice. Alternatively, it might be that mice and humans respond differently to heterozygous loss-of-function of this gene. We favor a third hypothesis—that human *ferroportin* mutations are not simple loss-of-function mutations and therefore not directly analogous to the situation in *Fpn*$^{null/+}$ mice. Mutations may not affect iron transport, per se, but rather perturb critical protein-protein interactions that might be cell type specific. Accordingly, it is interesting to note that no frameshift or termination codon mutations have been found among the many patients analyzed to date.

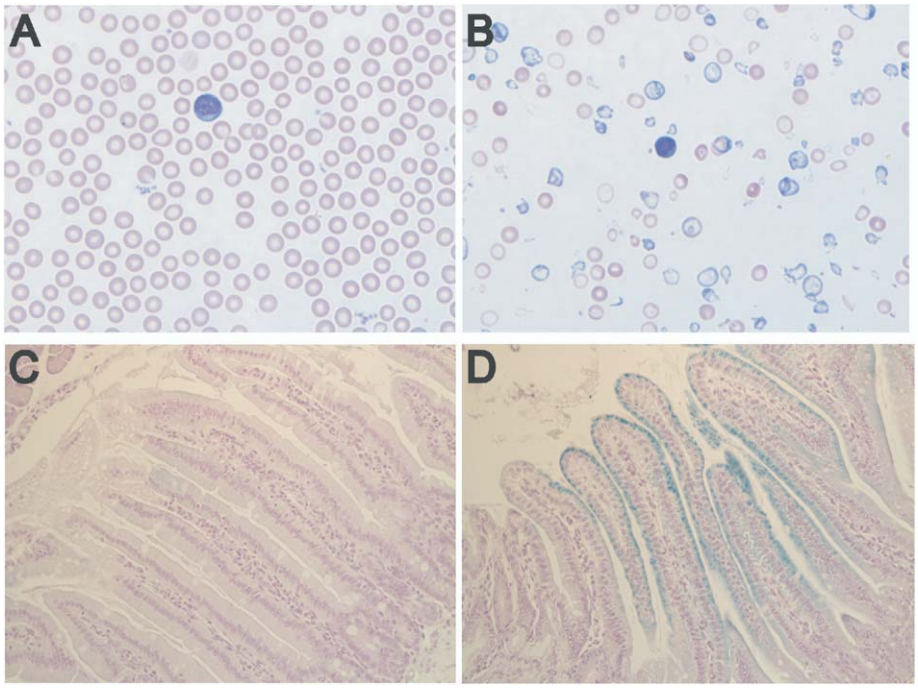

Figure 6. Ferroportin is critical for intestinal iron absorption

Wright-Giemsa-stained peripheral blood smears of tamoxifen-injected *Fpn*$^{flox/flox}$ (**A**) and *vil-Cre-ER*^{T2}; *Fpn*$^{flox/flox}$ (**B**) animals. Perls stain for nonheme iron in the duodenum of tamoxifen injected *Fpn*$^{flox/flox}$ (**C**) and *vil-Cre-ER*^{T2};*Fpn*$^{flox/flox}$ (**D**) animals. Blue staining represents nonheme iron accumulation in duodenal enterocytes.

These studies also explain why hepcidin deficiency results in clinical hemochromatosis. Hepcidin acts as a modulator of ferroportin function by triggering its degradation (Nemeth et al., 2004). Normally, increased iron availability stimulates hepcidin expression, probably triggering a homeostatic response in which hepcidin binds to ferroportin to cause its degradation. We can conclude that this is effective in controlling iron homeostasis because we have shown that ferroportin gates iron release at two key sites—in absorptive intestinal epithelial cells and recycling macrophages. We propose that, in hemochromatosis, perturbations in iron homeostasis result from a failure to control iron export through ferroportin, leading to increased iron release from macrophages and enhanced intestinal absorption.

Experimental Procedures

Targeted mutagenesis of *ferroportin*

Both the global and conditional targeting constructs modified a 15.5 kb KpnI fragment containing exons 4–8 of the mouse *ferroportin* genomic locus (Figure S1A). We used the pTKLNCL vector (originally from R. Mortenson). For the traditional targeting construct, the XhoI/BamHI fragment containing exon 6 and part of exon 7 was replaced by a 4.5 kb LoxP flanked cassette encoding a neomycin resistance gene and a cytosine deaminase gene. For the conditional targeting construct, the LoxP flanked cassette was inserted into an XhoI site in intron 5. A third LoxP site was inserted into an SphI site in intron 7 (Figure S1A). Coding sequence for thymidine kinase was also present in the pTKLNCL vector outside of the homology regions. The targeting constructs were introduced by electroporation into J1 embryonic stem cells (129 background), and cells were selected for resistance to G418 and ganciclovir. DNA samples from clones resistant to both G418 and ganciclovir were examined for homologous recombination by Southern blot analysis of HindIII digested DNA using a probe to exon 3 (Figures S1B and S1C). For each targeted allele (total knockout and conditional knockout), a single homologously recombined clone with a normal karyotype was injected into C57BL/6J mouse blastocysts, and these were transferred into the uteri of pseudopregnant females. High percentage male chimeras were bred with 129/SvEvTac females to generate F1 offspring carrying the modified *ferroportin* alleles. Germline transmission of the modified *ferroportin* alleles was determined by Southern blot analysis of tail DNA samples. For the conditional knockout model, we removed the neomycin resistance cassette from the targeted allele by mating to transgenic mice expressing Cre recombinase under control of the E2A promoter (Lakso et al., 1996). The E2A-Cre transgenic line had a 129/SvEvTac background.

Animals

Mice were maintained on standard mouse diet. Both the *Fpn* null and *Fpn*-floxed lines were maintained on the 129/SvEvTac background. For timed matings of *Fpn*$^{null/+}$ animals, the morning a plug was identified was considered E0.5. Plugged females were then sacrificed at E6.5 and later. Embryos were dissected from the uterus and either genotyped or used for immunohistochemistry. The *Meox2-Cre* mouse strain was obtained from the Jackson Laboratory (Bar Harbor, ME) on a mixed B6.129S4 background (Tallquist and Soriano, 2000). The *vil-Cre-ER*^{T2} transgenic line was obtained on a mixed background of B6/D2 and BL6 (el Marjou et al., 2004). The *Meox2-Cre* and *vil-Cre-ER*^{T2} mice were mated to *Fpn*$^{flox/+}$ animals to create *Meox2-Cre*; *Fpn*$^{flox/+}$ and *vil-Cre-ER*^{T2}; *Fpn*$^{flox/+}$ mice. Since *Meox2-Cre* can cause deletion in the germline, we also obtained *Meox2-Cre*;*Fpn*$^{null/+}$ mice from these crosses. Mice with the three genotypes described above were subsequently mated to *Fpn*$^{flox/flox}$ animals to create the animals that were studied in these experiments. Administration of tamoxifen to *Fpn*$^{flox/flox}$ and *vil-Cre-ER*^{T2}; *Fpn*$^{flox/flox}$ mice was performed once daily for 4 days starting between 7 and 10 days after birth. Tamoxifen (Sigma, St. Louis, MO) was first dissolved in 100% ethanol (50 mg/ml). Injection solution was prepared by diluting the tamoxifen to 8.3 mg/ml in sunflower seed oil (Sigma). Mice were weighed and injected with an amount of tamoxifen equal to 0.075 mg/g mouse. Mice were injected subcutaneously into the subscapular region with a single dose of either 1 mg or 5 mg of Fe-dextran (Watson Pharma, Morristown, NJ).

Southern blot and PCR genotyping

For Southern blot analysis, 10 μg of genomic DNA (Puregene Kit, Gentra Systems, Minneapolis, MN) was digested overnight with either HindIII or BamHI restriction enzyme, fractionated on a 0.5% TAE agarose gel, and transferred to Hybond N+ membrane (Amersham Biosciences, Piscataway, NJ). The probe for Southern blots was labeled by incorporation of ^{32}P-dCTP

into a PCR product amplified with the following primers: forward 5′-GCAATTTATTGGGTATAGCAG-3′ and reverse 5′-TGCCACCACCAGTCCATAGAC-3′. We genotyped mice by PCR analysis. *Fpn*$^{null/+}$ mice and embryos from intercrosses were genotyped using two PCR reactions. The wild-type allele (355 bp) was identified by amplification with the forward primer 5′-CTACACGTGCTCTCTTGAGAT-3′ (Xho5′) and the reverse primer 5′-GGTTAAACTGCTTCAAAGG-3′ (Xho3′). The targeted allele (359 bp) was identified by amplification with the same forward primer (Xho5′) and a reverse primer, 5′-GCCAAGTTCTAATTCCATCAG-3′, derived from the targeting vector. The *Fpn*$^{flox/+}$ and *Fpn*$^{flox/flox}$ mice were genotyped with one PCR reaction that had one forward primer (Xho5′) and two reverse primers, Xho3′ and 5′-CCTCATATGTGAGTCAAAGTATAG-3′. The wild-type allele generated a 355 bp band, and the floxed allele generated a 522 bp band. The band generated by full deletion with Cre recombinase was 398 bp. The *Meox2-Cre* mice were genotyped with primers that amplify Cre recombinase (200 bp): CREF (5′-CGTATAGCCGAAATTGCCAG-3′) and Cre-2-1 (5′-CAAAACAGGTAGTTATTCGG-3′). The *vil-Cre-ER*^{T2} mice were genotyped with the primers villin Cre-F (5′-CAAGCCTGGCTCGACGGCC-3′) and villin Cre-R (5′-CGCGAACATCTTCAGGTTCT-3′), resulting in a 300 bp band.

Immunohistochemistry

Immunohistochemistry of embryos was performed with a rabbit polyclonal anti-mouse ferroportin antibody elicited by injecting a fusion protein of glutathione S-transferase and 80 amino acids (residues 224–304) of mouse ferroportin protein into a New Zealand White rabbit. Antiserum was affinity purified against the same ferroportin peptide segment fused to dihydrofolate reductase using a preparative immunoblot procedure, as previously described (Canonne-Hergaux et al., 1999). Specificity to mouse ferroportin was confirmed by Western blot on membrane preparations from Madin-Darby canine kidney (MDCK) cells stably expressing ferroportin carrying a single missense mutation fused to green fluorescent protein at the C terminus (data not shown; F. Canonne-Hergaux, submitted). Embryos in their deciduum were fixed in 10% buffered formalin (Fisher Scientific, Fair Lawn, NJ) and embedded in paraffin. Sections were deparaffinized and heat treated for 30 min in 1.0 mM EDTA (pH 8.0) in an HS80 steamer (Black and Decker). Endogenous peroxidase activity was quenched with 3% aqueous hydrogen peroxide. Slides were then incubated in 3% normal swine serum in 0.05 M Tris (pH 7.6) followed by rabbit anti-ferroportin antibody (1:200 dilution) for 16 hr at room temperature. Slides were then incubated for 40 min with a horseradish peroxidase-labeled polymer conjugated to goat anti-rabbit immunoglobulin (EnVision+, Dako, Carpinteria, CA). Following antibody localization with 3.3′-diaminobenzidine tetrahydrochloride (DAB+, Dako), the stain was intensified by using a DAB enhancing solution (Zymed, South San Francisco, CA). Slides were counterstained with methyl green, dehydrated, and covered in Polymount (Poly Scientific, Bay Shore, NY). Immunohistochemistry on intestine sections was performed with a previously described polyclonal antibody against the C terminus of ferroportin (Donovan et al., 2000). The same procedure described above was followed, except that the antibody was incubated at a 1:400 dilution and for 1 hr.

Tissue iron staining and quantitative tissue iron measurements

Intestine, liver, and spleen samples were fixed in 10% buffered formalin and embedded in paraffin. Deparaffinized tissue sections were stained with the Perls Prussian blue stain for nonheme iron in the Children's Hospital Boston Pathology Laboratory. A subset of tissue sections was stained with a DAB-enhanced Perls iron stain (Dragatsis et al., 1998). Deparaffinized tissue sections were incubated for 30 min in 1% potassium ferrocyanide in 0.12N HCl. Endogenous peroxidase activity was quenched for 20 min at room temperature in 0.3% H_2O_2 in methanol. Sections were rinsed in PBS and incubated for 6 min in DAB/ H_2O_2 (DAB Plus Substrate Kit, Zymed). Quantitative measurement of nonheme iron was performed as described (Levy et al., 1999). Data is expressed as μg Fe/g wet weight of tissue.

Blood cell analysis

Mice were bled retroorbitally under anesthesia with 125–240 μg/kg avertin (Sigma). Blood smears were stained with Wright-Giemsa stain (Fisher Diagnostics, Middletown, VA). Blood for complete blood counts was collected into 600 μl EDTA anticoagulated microtainer tubes (Becton Dickenson, Franklin Lakes, NJ) and analyzed on an ADVIA 120 hematology analyzer (Bayer, Tarrytown, NY) with software specialized for mouse blood. Blood analysis was performed in the Clinical Core Laboratories at Children's Hospital Boston.

Statistics

We calculated all p values using Student's t test in Microsoft Excel.

Supplemental data

Supplemental Data include one figure and one table and can be found with this article online at http://www.cellmetabolism.org/cgi/content/full/1/3/191/DC1/.

Acknowledgments

This work was supported by P01 HL32262 (N.C.A.) and K01 5 K01 DK64924-02 (A.D.). N.C.A. is an investigator of the Howard Hughes Medical Institute. We thank Margaret Thompson and the Children's Hospital Mental Retardation Research Center Gene Manipulation Facility (NIH grant NIHP30-HD 18655) for ES cell transfections and blastocyst injections. We thank Vonnie Lee for technical assistance in the early stages of this project, Mark Fleming for help with immunohistochemistry, and Cameron Trenor for assistance with characterization of the mouse *ferroportin* genomic locus. We also thank Heiner Westphal for E2A-Cre transgenic mice and François Canonne-Hergaux and Philippe Gros for providing anti-ferroportin antiserum. The authors have no competing financial interests. The following are author contributions: A.D. and L.I.Z. enabled the knockout project by cloning and sequencing the mouse *ferroportin* genomic locus. A.D. and N.C.A. conceived and designed the experiments. A.D. performed the experiments to create the *ferroportin* mutant lines. A.D. and C.A.L. analyzed the knockout models. S.R. developed the villin-Cre mouse strains. G.S.P. and J.L.P. performed the immunohistochemistry experiments. A.D. and N.C.A. analyzed the data and wrote the manuscript.

Received: November 9, 2004
Revised: December 23, 2004
Accepted: January 6, 2005
Published: March 15, 2005

References

Abboud, S., and Haile, D.J. (2000). A novel mammalian iron-regulated protein involved in intracellular iron metabolism. J. Biol. Chem. *275*, 19906–19912.

Andrews, N.C. (2000). Iron homeostasis: insights from genetics and animal models. Nat. Rev. Genet. *1*, 208–217.

Bedard, Y.C., Pinkerton, P.H., and Simon, G.T. (1976). Uptake of circulating iron by the duodenum of normal mice and mice with altered iron stores, including sex-linked anemia: high resolution radioautographic study. Lab. Invest. *34*, 611–615.

Bielinska, M., Narita, N., and Wilson, D.B. (1999). Distinct roles for visceral endoderm during embryonic mouse development. Int. J. Dev. Biol. *43*, 183–205.

Bridle, K.R., Frazer, D.M., Wilkins, S.J., Dixon, J.L., Purdie, D.M., Crawford, D.H., Subramaniam, V.N., Powell, L.W., Anderson, G.J., and Ram, G.A. (2003). Disrupted hepcidin regulation in HFE-associated haemochromatosis and the liver as a regulator of body iron homoeostasis. Lancet *361*, 669–673.

Camaschella, C., Roetto, A., Cali, A., De Gobbi, M., Garozzo, G., Carella, M., Majorano, N., Totaro, A., and Gasparini, P. (2000). The gene TFR2 is mutated in a new type of haemochromatosis mapping to 7q22. Nat. Genet. *25*, 14–15.

Canonne-Hergaux, F., Gruenheid, S., Ponka, P., and Gros, P. (1999). Cellular and subcellular localization of the Nramp2 iron transporter in the intestinal brush border and regulation by dietary iron. Blood *93*, 4406–4417.

Canonne-Hergaux, F., Zhang, A.S., Ponka, P., and Gros, P. (2001). Characterization of the iron transporter DMT1 (NRAMP2/DCT1) in red blood cells of normal and anemic mk/mk mice. Blood *98*, 3823–3830.

Donovan, A., Brownlie, A., Zhou, Y., Shepard, J., Pratt, S.J., Moynihan, J., Paw, B.H., Drejer, A., Barut, B., Zapata, A., et al. (2000). Positional cloning of zebrafish ferroportin1 identifies a conserved vertebrate iron exporter. Nature *403*, 776–781.

Dragatsis, I., Efstratiadis, A., and Zeitlin, S. (1998). Mouse mutant embryos lacking huntingtin are rescued from lethality by wild-type extraembryonic tissues. Development *125*, 1529–1539.

el Marjou, F., Janssen, K.P., Chang, B.H., Li, M., Hindie, V., Chan, L., Louvard, D., Chambon, P., Metzger, D., and Robine, S. (2004). Tissue-specific and inducible Cre-mediated recombination in the gut epithelium. Genesis *39*, 186–193.

Feder, J.N., Gnirke, A., Thomas, W., Tsuchihashi, Z., Ruddy, D.A., Basava, A., Dormishian, F., Domingo, R., Ellis, M.C., Fullan, A., et al. (1996). A novel MHC class I-like gene is mutated in patients with hereditary haemochromatosis. Nat. Genet. *13*, 399–408.

Fleming, M.D., Trenor, C.C., Su, M.A., Foernzler, D., Beier, D.R., Dietrich, W.F., and Andrews, N.C. (1997). Microcytic anemia mice have a mutation in Nramp2, a candidate iron transporter gene. Nat. Genet. *16*, 383–386.

Fleming, M.D., Romano, M.A., Su, M.A., Garrick, L.M., Garrick, M.D., and Andrews, N.C. (1998). Nramp2 is mutated in the anemic Belgrade (b) rat: evidence of a role for Nramp2 in endosomal iron transport. Proc. Natl. Acad. Sci. USA *95*, 1148–1153.

Gunshin, H., Mackenzie, B., Berger, U.V., Gunshin, Y., Romero, M.F., Boron, W.F., Nussberger, S., Gollan, J.L., and Hediger, M.A. (1997). Cloning and characterization of a mammalian proton-coupled metal-ion transporter. Nature *388*, 482–488.

Hentze, M.W., Muckenthaler, M.U., and Andrews, N.C. (2004). Balancing acts: molecular control of mammalian iron metabolism. Cell *117*, 285–297.

Kawabata, H., Fleming, R.E., Gui, D., Moon, S.Y., Saitoh, T., O'Kelly, J., Umehara, Y., Wano, Y., Said, J.W., and Koeffler, H.P. (2005). Expression of hepcidin is down-regulated in TfR2 mutant mice manifesting a phenotype of hereditary hemochromatosis. Blood *105*, 376–381.

Knutson, M.D., Vafa, M.R., Haile, D.J., and Wessling-Resnick, M. (2003). Iron loading and erythrophagocytosis increase ferroportin 1 (FPN1) expression in J774 macrophages. Blood *102*, 4191–4197.

Lakso, M., Pichel, J.G., Gorman, J.R., Sauer, B., Okamoto, Y., Lee, E., Alt, F.W., and Westphal, H. (1996). Efficient in vivo manipulation of mouse genomic sequences at the zygote stage. Proc. Natl. Acad. Sci. USA *93*, 5860–5865.

Levy, J.E., Montross, L.K., Cohen, D.E., Fleming, M.D., and Andrews, N.C. (1999). The C282Y mutation causing hereditary hemochromatosis does not produce a null allele. Blood *94*, 9–11.

Liu, X.B., Hill, P., and Haile, D.J. (2002). Role of the ferroportin iron-responsive element in iron and nitric oxide dependent gene regulation. Blood Cells Mol. Dis. *29*, 315–326.

McKie, A.T., Marciani, P., Rolfs, A., Brennan, K., Wehr, K., Barrow, D., Miret, S., Bomford, A., Peters, T.J., Farzaneh, F., et al. (2000). A novel duodenal iron-regulated transporter, IREG1, implicated in the basolateral transfer of iron to the circulation. Mol. Cell *5*, 299–309.

Mok, H., Jelinek, J., Pai, S., Cattanach, B.M., Prchal, J.T., Youssoufian, H., and Schumacher, A. (2004). Disruption of ferroportin 1 regulation causes dynamic alterations in iron homeostasis and erythropoiesis in polycythaemia mice. Development *131*, 1859–1868.

Montosi, G., Donovan, A., Totaro, A., Garuti, C., Pignatti, E., Cassanelli, S., Trenor, C.C., Gasparini, P., Andrews, N.C., and Pietrangelo, A. (2001). Autosomal-dominant hemochromatosis is associated with a mutation in the ferroportin (SLC11A3) gene. J. Clin. Invest. *108*, 619–623.

Muckenthaler, M., Roy, C.N., Custodio, A.O., Minana, B., DeGraaf, J., Montross, L.K., Andrews, N.C., and Hentze, M.W. (2003). Regulatory defects in liver and intestine implicate abnormal hepcidin and Cybrd1 expression in mouse hemochromatosis. Nat. Genet. *34*, 102–107.

Nemeth, E., Tuttle, M.S., Powelson, J., Vaughn, M.B., Donovan, A., Ward, D.M., Ganz, T., and Kaplan, J. (2004). Hepcidin regulates cellular iron efflux by binding to ferroportin and inducing its internalization. Science *306*, 2090–2093.

Nemeth, E., Roetto, A., Garozzo, G., Ganz, T., and Camaschella, C. (2005). Hepcidin is decreased in TFR2-hemochromatosis. Blood *105*, 1803–1806. Published online October 14, 2004. 10.1182/blood-2004-08-3042

Nicolas, G., Bennoun, M., Devaux, I., Beaumont, C., Grandchamp, B., Kahn, A., and Vaulont, S. (2001). Lack of hepcidin gene expression and severe tissue iron overload in upstream stimulatory factor 2 (USF2) knockout mice. Proc. Natl. Acad. Sci. USA *98*, 8780–8785.

Nicolas, G., Bennoun, M., Porteu, A., Mativet, S., Beaumont, C., Grandchamp, B., Sirito, M., Sawadogo, M., Kahn, A., and Vaulont, S. (2002). Severe iron deficiency anemia in transgenic mice expressing liver hepcidin. Proc. Natl. Acad. Sci. USA *99*, 4596–4601.

Nicolas, G., Viatte, L., Lou, D.Q., Bennoun, M., Beaumont, C., Kahn, A., Andrews, N.C., and Vaulont, S. (2003). Constitutive hepcidin expression prevents iron overload in a mouse model of hemochromatosis. Nat. Genet. *34*, 97–101.

Njajou, O.T., Vaessen, N., Joosse, M., Berghuis, B., van Dongen, J.W., Breuning, M.H., Snijders, P.J., Rutten, W.P., Sandkuijl, L.A., Oostra, B.A., et al. (2001). A mutation in SLC11A3 is associated with autosomal dominant hemochromatosis. Nat. Genet. *28*, 213–214.

Papanikolaou, G., Samuels, M.E., Ludwig, E.H., MacDonald, M.L., Franchini, P.L., Dube, M.P., Andres, L., MacFarlane, J., Sakellaropoulos, N., Politou, M., et al. (2004). Mutations in HFE2 cause iron overload in chromosome 1q-linked juvenile hemochromatosis. Nat. Genet. *36*, 77–82.

Pietrangelo, A. (2004). The ferroportin disease. Blood Cells Mol. Dis. *32*, 131–138.

Roetto, A., Papanikolaou, G., Politou, M., Alberti, F., Girelli, D., Christakis, J., Loukopoulos, D., and Camaschella, C. (2003). Mutant antimicrobial peptide hepcidin is associated with severe juvenile hemochromatosis. Nat. Genet. *33*, 21–22.

Su, M.A., Trenor, C.C., Fleming, J.C., Fleming, M.D., and Andrews, N.C. (1998). The G185R mutation disrupts function of iron transporter Nramp2. Blood *92*, 2157–2163.

Tallquist, M.D., and Soriano, P. (2000). Epiblast-restricted Cre expression in MORE mice: a tool to distinguish embryonic vs. extra-embryonic gene function. Genesis *26*, 113–115.

Theiler, K. (1989). The House Mouse: Atlas of Embryonic Development (New York: Springer Verlag).

Tronche, F., Kellendonk, C., Kretz, O., Gass, P., Anlag, K., Orban, P.C., Bock, R., Klein, R., and Schutz, G. (1999). Disruption of the glucocorticoid receptor gene in the nervous system results in reduced anxiety. Nat. Genet. *23*, 99–103.